

## BLACK HOLES IN GALAXY MERGERS: EVOLUTION OF QUASARS

PHILIP F. HOPKINS<sup>1</sup>, LARS HERNQUIST<sup>1</sup>, THOMAS J. COX<sup>1</sup>, TIZIANA DI MATTEO<sup>2</sup>, PAUL MARTINI<sup>1</sup>, BRANT ROBERTSON<sup>1</sup>, VOLKER SPRINGEL<sup>2</sup>

*Submitted to ApJ April 06, 2005*

### ABSTRACT

Based on numerical simulations of gas-rich galaxy mergers, we discuss a model in which quasar activity is tied to the self-regulated growth of supermassive black holes in galaxies. The nuclear inflow of gas attending a galaxy collision triggers a starburst and feeds black hole growth, but for most of the duration of the starburst, the black hole is “buried”, being heavily obscured by surrounding gas and dust, limiting the visibility of the quasar, especially at optical and ultraviolet wavelengths. As the black hole grows, feedback energy from accretion heats the gas and eventually expels it in a powerful wind, leaving behind a “dead quasar”. In between the buried and dead phases, there is a window in time during which the galaxy would be seen as a luminous quasar. Because the black hole mass, radiative output, and distribution of obscuring gas and dust all evolve strongly with time, the duration of this phase of observable quasar activity depends on both the waveband and imposed luminosity threshold. We determine the observed and intrinsic lifetimes as a function of luminosity and frequency, and calculate observable lifetimes  $\sim 10$  Myr for bright quasars in the optical B-band, in good agreement with empirical estimates and much smaller than our estimated black hole growth timescales  $\sim 100$  Myr, naturally producing a substantial population of buried quasars. However, the observed and intrinsic energy outputs converge in the IR and hard X-ray bands as attenuation becomes weaker and chances of observation greatly increase. We also obtain the distribution of column densities along sightlines in which the quasar is seen above a given luminosity, and find that our result agrees remarkably well with observed estimates of the column density distribution from the SDSS for the appropriate luminosity thresholds. Our model reproduces a wide range of quasar phenomena, including observed quasar lifetimes, intrinsic lifetimes, column density distributions, and differences between optical and X-ray samples, having properties consistent with observations across more than five orders of magnitude in bolometric luminosity from  $10^9 - 10^{14} L_{\odot}$  ( $-17 \lesssim M_B \lesssim -30$ ).

*Subject headings:* quasars: general — galaxies: nuclei — galaxies: active — galaxies: evolution — cosmology: theory

### 1. INTRODUCTION

More than 40 years have passed since the recognition that quasars are at cosmological distances (Schmidt 1963; Greenstein & Mathews 1963; Mathews & Sandage 1963) and hence must be powerful energy sources. A combination of arguments based on time variability and energetics strongly supports the view that the activity is produced by the accretion of gas onto supermassive black holes in the centers of galaxies (e.g. Salpeter 1964; Zel’dovich & Novikov 1964; Lynden-Bell 1969). However, the mechanism that provides the trigger to fuel quasars remains uncertain. Recent discoveries of correlations between masses of black holes in nearby galaxies and either the mass (Magorrian et al. 1998) or velocity dispersion (i.e. the  $M_{\text{BH}}-\sigma$  relation: Ferrarese & Merritt 2000; Gebhardt et al. 2000) of spheroids demonstrate a fundamental link between the growth of supermassive black holes and galaxy formation. However, theoretical evidence connecting the origin of supermassive black holes and quasars to galaxy evolution remains elusive, owing to the complexity of the underlying physics and dynamics. In particular, up to now there has been no comprehensive model to explain the origin and fueling of quasars, or their lifetimes, obscuration, demographics, self-regulation and termination, and dependence on host galaxy properties.

Observations of the nearby Universe suggest that rapid

black hole growth may be related to massive flows of gas into the centers of galaxies. Infrared (IR) luminous galaxies represent the dominant population of objects above  $10^{11} L_{\odot}$  locally and it is believed that much of their IR emission is powered by dust reprocessing of radiation from intense nuclear starbursts (e.g. Soifer et al. 1984a,b; Sanders et al. 1986, 1988a,b; for a review, see e.g. Soifer et al. 1987). At the highest luminosities above  $10^{12} L_{\odot}$ , characteristic of ultraluminous infrared galaxies (ULIRGs), nearly all the galaxies appear to be in advanced stages of merging (e.g. Allen et al. 1985; Joseph & Wright 1985; Armus et al. 1987; Kleinmann et al. 1988; for reviews, see Sanders & Mirabel 1996 and Jögee 2004) and CO observations show that they contain large quantities of gas in their nuclei (e.g. Scoville et al. 1986; Sargent et al. 1987, 1989). Some ULIRGs exhibit “warm” IR spectral energy distributions, perhaps indicative of a buried quasar (e.g. Sanders et al. 1988c). This fact, together with the overlap between bolometric luminosities of ULIRGs and quasars, led Sanders et al. (1988a) to propose that quasars are the descendants of an infrared luminous phase of galaxy evolution caused by mergers. This scenario is supported by recent X-ray observations which have revealed the presence of two non-thermal point sources near the center of the ULIRG NGC6240 (Komossa et al. 2003), which are most naturally interpreted as accreting supermassive black holes that are heavily obscured at visual wavelengths (e.g. Gerssen et al. 2004; Max et al. 2005).

Hydrodynamic simulations have shown that gas inflows are produced by strong gravitational torques on the gas through tidal forces during mergers involving gas-rich galaxies (e.g.,

<sup>1</sup> Harvard-Smithsonian Center for Astrophysics, 60 Garden Street, Cambridge, MA 02138, USA

<sup>2</sup> Max-Planck-Institut für Astrophysik, Karl-Schwarzschild-Straße 1, 85740 Garching bei München, Germany

Hernquist 1989; Barnes & Hernquist 1991, 1996). The resulting dense concentrations of gas in the inner regions of the remnant can sustain star formation at rates high enough and for sufficiently long timescales to account for many properties of ULIRGs (e.g., Mihos & Hernquist 1994, 1996; Hernquist & Mihos 1995). However, these authors were not able to directly explore the relationship between the gas inflows and quasar activity because their simulations did not include a model for black hole growth and the impact of strong feedback from either star formation or quasars.

One of the most fundamental parameters of black hole growth is the quasar lifetime,  $t_Q$ , which sets the timescale for the most luminous phase of the activity. Observations generally constrain quasar lifetimes to the range  $t_Q \approx 10^6 - 10^8$  yr (for a review, see Martini 2004). These estimates are primarily based on demographic or integral arguments which combine observations of the present-day population of supermassive black holes and accretion by the high-redshift quasar population (e.g., Soltan 1982; Haehnelt, Natarajan, & Rees 1998; Yu & Tremaine 2002; Yu & Lu 2004), or incorporate quasars into models of galaxy evolution (e.g., Kauffmann & Haehnelt 2000; Wyithe & Loeb 2002; Di Matteo et al. 2003, 2004; Granato et al. 2004) or reionization of HeII (e.g. Sokasian et al. 2002, 2003). Results from clustering in quasar surveys (e.g., Porciani, Magliocchetti, & Norberg 2004; Grazian et al. 2004), the proximity effect in the Ly $\alpha$  forest (Bajtlik, Duncan & Ostriker 1988; Haiman & Cen 2002; Yu & Lu 2005; although such results may still be inconclusive, e.g. Croft 2004), and the transverse proximity effect in He II (Jakobsen et al. 2003) similarly suggest lifetimes  $t_Q \sim 10^7$  yr.

It is not immediately obvious how quasar lifetimes  $t_Q \sim 10^7$  yr can be explained in the context of gas inflows triggered by galaxy mergers. The full duration of the starburst phase is set by the timescale during which strong gas inflows are excited, which in turn is determined by the time when significant gravitational torques are exerted on the gas. The numerical simulations of Mihos & Hernquist (1994, 1996) showed that this occurs for  $\sim 2 \times 10^8$  yr, much shorter than typical merger timescales of  $> 10^9$  yr (Barnes 1988, 1992; Hernquist 1992, 1993), but in good agreement with observed estimates for the gas depletion time in the central regions of ULIRGs (for a discussion, see e.g. Barnes & Hernquist 1992). If gas-rich mergers are indeed responsible for the origin of quasar activity, as suggested through studies of ULIRGs (e.g. Sanders et al. 1988a) and more directly from observations of quasar hosts (e.g. Stockton 1978; Heckman et al. 1984; Stockton & MacKenty 1987; Stockton & Ridgway 1991; Hutchings & Neff 1992; Bahcall et al. 1994, 1995; Canalizo & Stockton 2001), the factor  $\sim 10$  difference between the gas consumption time in ULIRGs and quasar lifetimes must be reconciled.

Semi-analytical models of supermassive black hole evolution and its correlation with galaxy structure suggest that, beyond a certain threshold, feedback energy expels nearby gas and shuts down the accretion phase (Ciotti & Ostriker 1997, 2001; Silk & Rees 1998; Fabian 1999; Wyithe & Loeb 2003). However, these calculations provide only limits, and in neglecting the dynamics of quasar evolution they do not predict time-dependent effects such as the characteristic lifetime of the accretion phase prior to its self-termination, the fueling rates for black hole accretion, the obscuration of central sources, or the quasar light curve. These quantities are instead usually taken to be independent input parameters of the model. For example, the lifetime is either adopted from obser-

vational estimates or assumed to be similar to a characteristic timescale such as the dynamical time of the host galaxy disk or the  $e$ -folding time for Eddington-limited black hole growth  $t_S = M_{\text{BH}}/\dot{M} = 4.5 \times 10^7 l (\epsilon_r/0.1) \text{ yr}$  for accretion with radiative efficiency  $\epsilon_r = L/\dot{M}c^2 \sim 0.1$  and  $l = L/L_{\text{Edd}} \lesssim 1$  (Salpeter 1964).

Recently, Springel et al. (2005b) have developed a methodology for incorporating black hole growth and feedback into hydrodynamical simulations of galaxy mergers that includes a multiphase model for star formation and pressurization of the interstellar gas by supernova feedback (Springel & Hernquist 2003). Using this approach, we have begun to explore the impact of these processes on galaxy formation and evolution. Di Matteo et al. (2005) and Springel et al. (2005b) have shown that the gas inflows produced by gravitational torques during a merger both trigger starbursts (as in the earlier simulations of e.g. Mihos & Hernquist 1994, 1996) and fuel rapid black hole growth. The growth of the black hole is determined by the gas supply and terminates abruptly when significant gas is expelled owing to the coupling between feedback energy from black hole accretion and the surrounding gas. Eventually, as the gas is heated and driven out, the remnant is no longer active because the black hole does not accrete at a high rate, leaving a dead quasar in an ordinary galaxy. The self-regulated nature of the black hole growth explains observed correlations between black hole mass and properties of normal galaxies (Di Matteo et al. 2005), as well as the color distribution of ellipticals (Springel et al. 2005a). These results lend support to the view that mergers have played an important role in structuring galaxies, as advocated by e.g. Toomre & Toomre (1972) and Toomre (1977).

Moreover, Di Matteo et al. (2005) showed that the dynamics of the inflowing gas and its response to the self-regulated growth of the black hole yield a timescale for the strong accretion phase  $\sim 2 \times 10^8$  yr, comparable to the full duration of the starburst. During much of this period, the bolometric luminosity of the black hole would exceed the threshold to be classified as a quasar, implying a timescale  $\sim 10^8$  yr (for a Milky Way mass system) for the intrinsic quasar phase of the black hole.

In Hopkins et al. (2005a), we employed models for obscuration by gas and dust to show that for most of the accretion lifetime the quasars would be buried; i.e. heavily obscured by the large gas density powering accretion. Eventually, feedback from the accretion energy drives away the gas, creating a brief window in which the central object would be observable as an optical quasar, until accretion levels drop below quasar thresholds. By calculating the effects of obscuration from the simulation of a merger of gas-rich galaxies, we showed that this determines an observable lifetime  $\sim 10^7$  yr, in good agreement with observations.

Here, we extend and further develop implications of the model for quasar evolution proposed in Hopkins et al. (2005a) by analyzing a series of hydrodynamical simulations of galaxy mergers where we vary the masses of the progenitor galaxies, so that they have virial velocities between 80 and  $320 \text{ km s}^{-1}$ . In §2 we describe our series of merger simulations and the calculation of column densities and obscuration, and compare the results obtained with different column density calculations. In §3 we examine the frequency dependence of our results and quantify the differences in lifetimes across the optical and X-ray bands. In §4 we examine the typical column densities along lines-of-sight to the simulated quasars,

TABLE 1  
SIMULATION PARAMETERS

Simulation	$V_{\text{vir}}$ (km s $^{-1}$ )	$M_{\text{vir}}$ ( $M_{\odot}$ )	$M_{\text{BH, final}}$ ( $M_{\odot}$ )
A1	80	$1.7 \times 10^{11}$	$7 \times 10^6$
A2	113	$4.8 \times 10^{11}$	$3 \times 10^7$
A3	160	$1.4 \times 10^{12}$	$3 \times 10^8$
A4	226	$3.8 \times 10^{12}$	$7 \times 10^8$
A5	320	$1.1 \times 10^{13}$	$2 \times 10^9$

and compare these to observed distributions from both optical and X-ray surveys. In §5 we show the simulation results for our merger series and compare the observed and intrinsic lifetimes as a function of luminosity for all the simulations. Finally, in §6 we discuss our results and the implications of our model for a broad range of quasar studies.

## 2. THE MODEL: CALCULATIONS

### 2.1. The Simulations

The simulations were performed using the GADGET-2 code, a new version of the parallel TreeSPH code GADGET (Springel, Yoshida, & White 2001). It uses an entropy-conserving formulation (Springel & Hernquist 2002) of smoothed particle hydrodynamics (SPH), and includes radiative cooling, heating by a UV background (as described in e.g. Katz et al. 1996; Davé et al. 1999), and a sub-resolution model of a multiphase interstellar medium (ISM) to describe star formation and supernova feedback (Springel & Hernquist 2003). This sub-resolution model provides an effective equation of state for star-forming gas which includes pressure feedback from supernova heating, and allows us to stably evolve even massive pure gas disks (see, e.g. Springel et al. 2005b; Robertson et al. 2004). The methodology of accretion, feedback, and galaxy generation is described in detail in Springel et al. (2005b).

In our approach, supermassive black holes (BHs) are represented by “sink” particles that accrete gas from their local environment, with an accretion rate  $\dot{M}$  estimated from the local gas density and sound speed using a Bondi-Hoyle-Lyttleton parameterization with an imposed upper limit equal to the Eddington rate. The bolometric luminosity of the BH particle is then  $L_{\text{bol}} = \epsilon_r \dot{M} c^2$ , where  $\epsilon_r = 0.1$  is the radiative efficiency. We further assume that a small fraction (5%) of  $L_{\text{bol}}$  couples dynamically to the surrounding gas, and that this feedback is injected into the gas as thermal energy. This fraction is a free parameter, determined in Di Matteo et al. (2005) by fitting to the  $M_{\text{BH}}-\sigma$  relation. We do not attempt to resolve the small-scale accretion dynamics near the black hole, but instead assume that the time-averaged accretion can be estimated from the gas properties on the scale of our spatial resolution ( $\lesssim 50$  pc).

In what follows, we analyze five simulations of colliding disk galaxies, which form a family of structurally similar models with different virial velocity and mass. In each simulation, we generate two stable, isolated disk galaxies, each with an extended dark matter halo with a Hernquist (1990) profile, motivated by cosmological simulations (e.g. Navarro et al. 1996; Busha et al. 2004) and observations of halo properties (e.g. Rines et al. 2002, 2002, 2003, 2004), an exponential gas disk, and a bulge. The simulations follow the series described in detail in Springel et al. (2005a), with

the parameters listed in Table 1. We denote the simulations A1, A2, A3, A4, and A5, with increasing virial velocities of  $V_{\text{vir}} = 80, 113, 160, 226,$  and  $320$  km s $^{-1}$ , respectively. Note that the self-similarity of these models is broken by the scale-dependent physics of cooling, star formation, and black hole accretion. In Hopkins et al. (2005a), we describe our analysis of simulation A3, a fiducial choice with a rotation curve and mass similar to the Milky Way. The galaxies have mass  $M_{\text{vir}} = V_{\text{vir}}^3 / (10GH_0)$ , with the baryonic disk having mass fraction  $m_{\text{d}} = 0.041$ , the bulge  $m_{\text{b}} = 0.0136$ , and the rest of the mass in dark matter with a concentration parameter 9.0. The disk-scale length is computed based on an assumed spin parameter  $\lambda = 0.033$ , and the scale-length of the bulge is set to 0.2 times this. We begin our simulation with pure gas disks, which may better correspond to the high-redshift galaxies in which most quasars are observed.

Each galaxy is initially composed of 168000 dark matter halo particles, 8000 bulge particles, 24000 gaseous disk particles, and one BH particle, with a small initial seed mass of  $10^5 M_{\odot}$ . Given these choices, the dark matter, gas, and star particles are all of roughly equal mass, and central cusps in the dark matter and bulge profiles are reasonably well resolved (see Fig 2. in Springel et al. 2005b). The galaxies are then set to collide in a prograde encounter with zero orbital energy and a small pericenter separation (7.1 kpc for the A3 simulation).

### 2.2. Column Densities & Quasar Attenuation

We calculate the column density between a black hole and a hypothetical observer from the simulation outputs spaced every 10 Myr before and after the merger and every 5 Myr during the merger of each galaxy pair. The calculation method is described in Hopkins et al. (2005a), but we review it briefly here. We generate  $\sim 1000$  radial lines-of-sight (rays), each with its origin at the black hole particle location and with directions uniformly spaced in solid angle  $d \cos \theta d\phi$ . For each ray, we then begin at the origin, calculate and record the local gas properties using GADGET, and then move a distance along the ray  $\Delta r = \eta h_{\text{sml}}$ , where  $\eta \leq 1$  and  $h_{\text{sml}}$  is the local SPH smoothing length. The process is repeated until a ray is sufficiently far from its origin ( $\gtrsim 100$  kpc). The gas properties along a given ray can then be integrated to give the line-of-sight column density and mean metallicity. We test different values of  $\eta$  and find that gas properties along a ray converge rapidly and change smoothly for  $\eta = 0.5$  and smaller. We similarly test different numbers of rays and find that the distribution of line-of-sight properties converges for  $\gtrsim 100$  rays.

Given the local gas properties, we use the GADGET multiphase model of the ISM described in Springel & Hernquist (2003) to calculate the local mass fraction in “hot” (diffuse) and “cold” (molecular and HI cloud core) phases of dense gas and, assuming pressure equilibrium between the two phases, we obtain the local density of the hot and cold phase gas and the corresponding volume filling factors. The values obtained correspond roughly to the fiducial values of McKee & Ostriker (1977). Given a temperature for the warm, partially ionized component  $\sim 8000$  K, determined by pressure equilibrium, we further calculate the neutral fraction of this gas, typically  $\sim 0.3 - 0.5$ . We denote the neutral and total column densities as  $N_{\text{HI}}$  and  $N_{\text{H}}$ , respectively. Using only the hot-phase density allows us to place an effective lower limit on the column density along a particular line of sight, as it assumes a ray passes only through the diffuse ISM, with  $\gtrsim 90\%$  of the mass of the dense ISM concentrated in cold-phase “clumps.” Given the small volume filling factor

(< 0.01) and cross section of such clouds, we expect that the majority of sightlines will pass only through the “hot-phase” component.

Using  $L_{\text{bol}} = \epsilon_r \dot{M} c^2$ , we model the form of the intrinsic quasar continuum SED following Marconi et al. (2004), based on optical through hard X-ray observations (e.g., Elvis et al. 1994; George et al. 1998; Vanden Berk et al. 2001; Perola et al. 2002; Telfer et al. 2002; Ueda et al. 2003; Vignali et al. 2003). This gives a B-band luminosity  $\log(L_B) = 0.80 - 0.067\mathcal{L} + 0.017\mathcal{L}^2 - 0.0023\mathcal{L}^3$ , where  $\mathcal{L} = \log(L_{\text{bol}}/L_\odot) - 12$ , and we take  $\lambda_B = 4400\text{\AA}$ . We then use a gas-to-dust ratio to determine the extinction along a given line of sight at this frequency. Observations suggest that the majority of the population of reddened quasars have reddening curves similar to that of the Small Magellanic Cloud (SMC; Hopkins et al. 2004), which has a gas-to-dust ratio lower than the Milky Way by approximately the same factor as its metallicity (Bouchet et al. 1985). We therefore consider both a gas-to-dust ratio equal to that of the Milky Way,  $(A_B/N_{\text{HI}})_{\text{MW}} = 8.47 \times 10^{-22} \text{ cm}^2$ , and a gas-to-dust ratio scaled by metallicity,  $A_B/N_{\text{HI}} = (Z/0.02)(A_B/N_{\text{HI}})_{\text{MW}}$ . For both cases we use the SMC-like reddening curve of Pei (1992). We calculate extinction in X-ray frequencies (0.03–10 keV) using the photoelectric absorption cross sections of Morrison & McCammon (1983) and non-relativistic Compton scattering cross sections, similarly scaled by metallicity. In determining the column density for photoelectric X-ray absorption, we ignore the inferred ionized fraction of the gas, as it is expected that the inner-shell electrons which dominate the photoelectric absorption edges will be unaffected in the temperature ranges of interest. We do not perform a full radiative transfer calculation, and therefore do not model scattering or re-processing of radiation by dust in the infrared.

### 2.3. Quasar Lifetimes & Sensitivity to Simulation Parameters

We quantify the quasar lifetime  $t_Q$  as in Hopkins et al. (2005a), as a function of the limiting B-band luminosity  $L_{B,\text{min}}$ . For each sightline, an observed lifetime is determined as the integrated time in the simulation during which the given sightline sees a B-band luminosity above a given threshold,  $L_{B,\text{obs}} > L_{B,\text{min}}$ . We consider both the intrinsic lifetime  $t_Q^i$ , the total time the intrinsic  $L_B \geq L_{B,\text{min}}$  (ignoring attenuation), and the observed lifetime derived from a particular column density calculation. We note that below 5 Myr (the simulation output frequency in the standard case) our estimates of  $t_Q$  become uncertain owing to the effects of quasar variability and our inability to resolve the local small-scale physics of the ISM. However, the majority of sightlines see lifetimes in the range 10–20 Myr up to  $L_{B,\text{min}} = 10^{11} L_\odot$ , in good agreement with observations suggesting lifetimes  $\sim 10^7$  yr and well above this limit.

Figure 1 shows the lifetime obtained in the A3 simulation using different calculations of the column density  $N_{\text{HI}}$  (cases A–D). The uppermost curve in all cases is the intrinsic lifetime  $t_Q^i$ . The lower thick curve is the median observed lifetime calculated using a particular estimate of the column density, with the thin curves representing the 25%–75% inclusion contours. The cold-phase ISM density (A) is large enough for the quasar to be completely extinguished out of observable ranges for the duration of the quasar phase, rendering the object observable only during quiescent phases with  $L_B \sim 10^9 L_\odot$ . We also show the significantly longer lifetimes calculated using the hot-phase ISM density, first ignoring corrections for metallic-

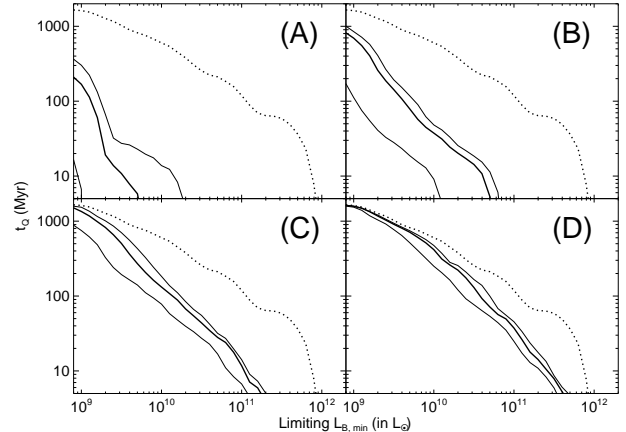


FIG. 1.— Quasar lifetimes as a function of  $L_{B,\text{min}}$  from the A3 simulation. The dotted lines show the lifetime if attenuation is ignored (time with observed B-band luminosity  $L_{B,\text{obs}} \geq L_{B,\text{min}}$ ). The thick solid lines indicate the median observed lifetime, with thin lines giving the 25%–75% contours. Lifetimes are calculated using: (A) cold-phase ISM density, (B) hot-phase density (ignoring metallicity and ionization), (C) hot-phase density (including metallicity and ionization), (D) hot-phase density with artificially low metallicity (0.1 times solar).

ity and ionization (B; i.e. assuming  $A_B/N_{\text{HI}} = (A_B/N_{\text{HI}})_{\text{MW}}$  and  $N_{\text{HI}} = N_{\text{H}}$ ) and then including these effects (C), which increases the median lifetime by a factor  $\sim 2$  and significantly reduces the scatter towards shorter lifetimes. Finally, we calculate the lifetime using the hot-phase density and an SMC-like gas-to-dust ratio,  $(A_B/N_{\text{HI}})_{\text{SMC}} = 0.869 \times 10^{-22} \text{ cm}^2$  (D; essentially assuming a metallicity 0.1 times solar), which sets a strong upper limit on the observed lifetime. These lifetimes are still only  $\sim 2$  times as long as the lifetimes calculated using metallicity-weighted neutral column densities, and still  $\sim 1/3$  the intrinsic lifetime at  $L_{B,\text{min}} = 10^{11} L_\odot$ . We therefore expect that, after accounting for the clumping of most mass in the cold phase of the most dense regions of the ISM, the qualitative relation between our observed and intrinsic calculated lifetimes should be relatively insensitive to the details of the column density calculation, with variation by a factor of  $\sim 2 - 3$  between lifetimes calculated using different prescriptions for the multiphase ISM, ionization, and metallicity effects.

### 3. FREQUENCY DEPENDENCE OF THE QUASAR LIFETIME

We expect the intrinsic quasar lifetime above a given luminosity in a particular band to change with the frequency of that band. The shift in lifetime with frequency is approximately given by an offset in luminosity corresponding to the difference in luminosities at different frequencies in our model quasar spectrum. However, this change is not entirely history-independent, as the model spectrum alters shape with varying luminosity owing to bolometric corrections. More important, our model predicts that the observed lifetime above a given luminosity will change with frequency not only as a result of the shift in intrinsic lifetime, but primarily as a result of varying levels of attenuation at different frequencies.

Figure 2 shows the lifetimes as a function of luminosity for the A3 simulation, for various frequencies in the optical and X-ray bands. We plot lifetimes in the manner of Figure 1; i.e. the total time with  $\nu L_\nu > L_{\nu,\text{min}}$  ( $L_{\nu,\text{min}} \equiv (\nu dL/d\nu)_{\text{min}}$ ), at the representative optical wavelengths  $\lambda = 3000, 4500, 6000, 7500, \text{ and } 9000\text{\AA}$  (colored black to blue to

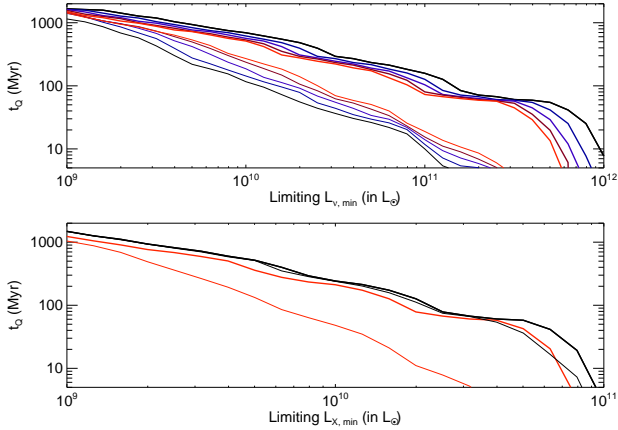


FIG. 2.— Quasar lifetimes as a function of  $L_{B,min}$  from the A3 simulation, showing the waveband dependence of the lifetime. The thick lines give the lifetime if attenuation is ignored, thin lines indicate the median observed lifetime (calculated using the metallicity-weighted, hot-phase neutral column density). Upper panel: From black to blue to red, lifetimes are calculated at 3000, 4500, 6000, 7500, and 9000 Å. Lower panel: lifetimes are calculated for soft (0.5 – 2 keV, red) and hard (2 – 10 keV, black) X-ray bands.

red, respectively). We find that the intrinsic lifetime systematically decreases at longer wavelengths (based on the shape of the quasar SED), while the observed lifetime increases (owing to weakening attenuation), with the two approaching one another near infrared wavelengths. At longer wavelengths, we expect the curves to cross, as the observed lifetime in the far IR, owing to dust re-processing of quasar radiation, will be longer than the intrinsic lifetime, but we do not yet incorporate such re-processing into our column density calculations. At very low  $L_{\nu,min}$ , lifetimes approximately converge to the total duration of the simulations, as the quasar is above such luminosities throughout almost the entire merger.

The lower panel of Figure 2 shows the lifetimes in the soft and hard X-ray bands, defined as 0.5 – 2 keV and 2 – 10 keV, respectively. We find that the soft X-ray band is heavily attenuated and has much shorter observed than intrinsic lifetimes, primarily owing to photoelectric absorption. However, the hard X-ray band is relatively unaffected, as the hot-phase column densities tend to be well below the Compton-thick regime  $N_H \sim 10^{24} \text{ cm}^{-2}$ . Thus, most quasars obscured in the optical for much of their high accretion rate lifetimes should be observable in hard X-rays. We defer a full treatment of the difference between the attenuation of soft and hard X-rays to a future paper, but note that this difference may account for the slope of the cosmic X-ray background, with a population of obscured quasars at spectral energies  $\lesssim$  a few keV as a natural stage in the evolution of quasar activity.

#### 4. TYPICAL COLUMN DENSITIES

Given a calculation of the column density along multiple lines-of-sight to the simulated quasars, we can examine the typical column density distributions at all times and at times in which the quasar is observed above some luminosity threshold. Following the analysis in Hopkins et al. (2005a), we expect the characteristic column densities to rise rapidly during the merger, as gas inflow traces and fuels a rising accretion rate. Eventually, column densities rapidly fall in a blowout phase once the black hole has reached a critical mass, creating a window with rapidly changing column densities in which the quasar is observable until accretion rates drop below those

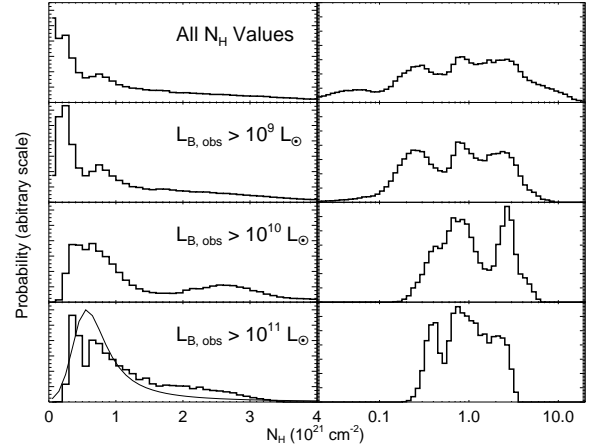


FIG. 3.— Distribution of “hot-phase”, neutral column densities  $N_{\text{HI}}$  from the A3 simulation. The probability of seeing a given  $N_{\text{HI}}$  is weighted by the time such an  $N_{\text{HI}}$  is observed along all sightlines. Plots are scaled linearly (left) and logarithmically (right). The top panel shows all  $N_{\text{HI}}$  values from all times, the lower panels give the distribution for times where the observed B-band luminosity is above the  $L_{B,min}$  shown. The smooth curve is the distribution of  $N_{\text{HI}}$  values from the observed SDSS quasar sample of Hopkins et al. (2004), who used an absolute  $i$ -band magnitude limit approximately equivalent to  $L_{B,obs} > 10^{11} L_{\odot}$ , scaled to the appropriate modal  $N_{\text{HI}}$ .

necessary to fuel quasar activity. As is clear in Figure 2 of Hopkins et al. (2005a), the dispersion in  $N_{\text{HI}}$  at any particular time in the simulation is generally small, a factor of  $\sim 2$  in either direction, but typical  $N_{\text{HI}}$  values can change by an order of magnitude over timescales  $\sim$  Myr. Therefore, it is of interest to consider the probability of an observer, viewing the object at a random time, seeing a given column density.

Figure 3 plots the distribution of column densities  $N_{\text{HI}}$  calculated using the hot-phase metallicity-weighted ISM density in the A3 simulation. The probability of seeing a given  $N_{\text{HI}}$  is calculated as proportional to the total time along all sightlines that such an  $N_{\text{HI}}$  is observed. The plots are scaled both linearly (left panels) and logarithmically (right panels) in column density. Typical column densities are distributed about  $N_{\text{HI}} = 10^{21} \text{ cm}^{-2}$ , approximately symmetrically in  $\log N_{\text{HI}}$ . We further plot the distribution of  $N_{\text{HI}}$  values requiring that the observed B-band luminosity be above some threshold  $L_{B,min}$ . The curve shown in the linear plots is the best-fit to the  $E_{B-V}$  distribution of bright SDSS quasars with  $z < 2.2$ , from Hopkins et al. (2004). The curve has been rescaled in terms of the column density (inverting our gas-to-dust prescription) and plotted about a peak (mode)  $N_{\text{HI}}$  (undetermined in Hopkins et al. 2004) of  $N_{\text{HI}} \approx 0.5 \times 10^{21} \text{ cm}^{-2}$ . The  $i$ -band absolute magnitude limit imposed in the observed sample,  $M_i < -22$ , corresponds approximately to our plotted B-band limit  $L_{B,obs} > 10^{11} L_{\odot}$ .

The agreement between the observed column density distribution and the result of our simulations once the same selection effect is applied is strong evidence in favor of our model for quasar evolution. The distribution as a function of limiting luminosity is a natural consequence of the dynamics of the quasar activity. Throughout much of the duration of bright quasar activity, column densities rise to high levels as a result of the same process that feeds accretion, naturally producing a reddened population of quasars (a red “tail” in the quasar color distribution), extending to very bright quasars strongly reddened by large  $N_{\text{HI}}$ . The existence of

this extended reddened quasar population in radio and optically selected quasars is well known (e.g. Webster et al. 1995; Brotherton et al. 2001; Francis et al. 2001; Richards et al. 2001; Gregg et al. 2002; White et al. 2003), and we are able to reproduce its distribution not as a distribution of source properties but as a result of the time evolution of quasar phenomena. Our estimate of the distribution of  $N_{\text{HI}}$  for  $L_{B,\text{obs}} > 10^{11} L_{\odot}$  does not account for an additional selection effect, namely that strongly reddened quasars may not be extinguished from an observed sample (if the intrinsic luminosity is large enough), but their colors may be significantly reddened to the point where color selection criteria of quasar surveys will not include them. However, this effect would only serve to bring our distribution into better agreement with observations, as it would slightly lower the high- $N_{\text{HI}}$  tail.

Moreover, our estimates of the distribution of  $N_{\text{HI}}$  allow us to make a directly observable prediction, namely that the column density distribution in optically selected samples with a minimum absolute magnitude or luminosity should broaden in both directions (to larger and smaller  $N_{\text{HI}}$ ) as the limiting selection luminosity is decreased (limiting absolute magnitude increased). This is because, at lower luminosities, observers will see both intrinsically bright periods extinguished by larger column densities (broadening the distribution to larger  $N_{\text{HI}}$  values) and intrinsically faint periods with small column densities (broadening the distribution to smaller  $N_{\text{HI}}$  values). The distribution of  $N_{\text{H}}$  values in hard X-ray quasar samples, which are much less affected by this extinction (see §3), should also reflect this trend, and indeed the distribution of  $N_{\text{H}}$  values is much broader and flatter, with quasars seen from  $N_{\text{H}} \sim 10^{20} - 10^{24} \text{ cm}^{-2}$  (Ueda et al. 2003).

Extension of this distribution to the other black hole masses and peak quasar luminosities of our simulations reveals similar qualitative behavior. The characteristic column densities during the obscured, intrinsically bright phases of accretion generally increase with galaxy and black hole mass, but typically by factors  $\lesssim 10$  across the range of our simulations  $V_{\text{vir}} = 80 - 320 \text{ km s}^{-1}$ . Additionally, although mean column densities increase somewhat with increasing mass, the functional form of the  $N_{\text{HI}}$  distribution remains similar at each limiting luminosity, implying that a combined population of quasars similar to those we have simulated will match the observed  $N_{\text{HI}}$  distribution with appropriate selection effects accounted for as in Figure 3. Finally, we note that although we do not see extremely large column densities  $N_{\text{H}} \gtrsim 10^{24} \text{ cm}^{-2}$  in the distributions from our simulations, our model does not rule out such values. It is possible that very bright quasars in unusually massive galaxies or quasars in higher-redshift, compact galaxies which we have not simulated may, during peak accretion periods, reach such values in their typical column densities. Moreover, as our model assumes  $\sim 90\%$  of the mass of the densest gas is clumped into cold-phase molecular clouds, a small fraction of sightlines will pass through such clouds and encounter column densities similar to those shown for the cold phase in Figure 1, as large as  $N_{\text{H}} \sim 10^{26} \text{ cm}^{-2}$ . This also allows a large concentration of mass in sub-resolution obscuring structures, such as an obscuring toroid on scales  $\lesssim 100 \text{ pc}$ , although many of the phenomena such structures are invoked to explain can be accounted for through our model of time-dependent obscuration.

## 5. EXTENSION OF QUASAR LIFETIMES TO OTHER MASSES

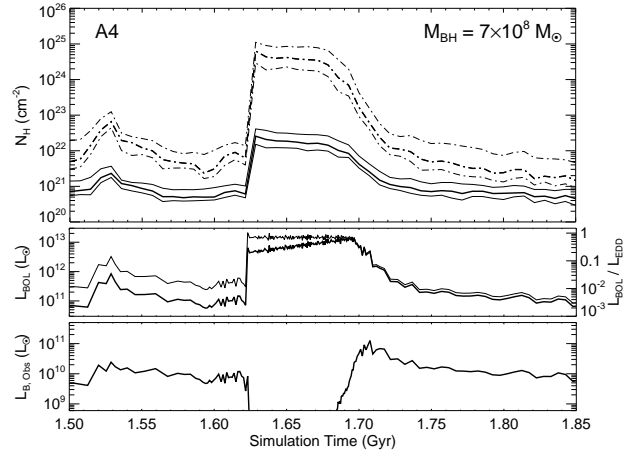


FIG. 4.— Upper panel: Thick contours plot the median column density  $N_{\text{H}}$  as a function of simulation time, with thin contours at 25% and 75% inclusion levels, for the A4 simulation ( $V_{\text{vir}} = 226 \text{ km s}^{-1}$ ). Solid contours represent the density of the “hot-phase” ISM, dashed contours the total simulation density. Middle panel: Bolometric luminosity of the black hole in the simulation,  $L_{\text{bol}} = \epsilon_r \dot{M} c^2$  (thick), and ratio of bolometric to Eddington luminosity,  $l \equiv L_{\text{bol}}/L_{\text{Edd}}$  (thin). Values are shown for each simulation timestep. Lower panel: Observed B-band luminosity with  $N_{\text{HI}}$  calculated using the median “hot-phase” ISM density.

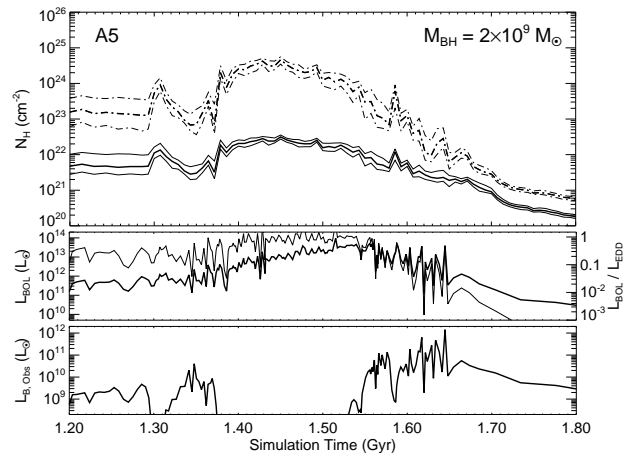


FIG. 5.— Same as Figure 4, but for the A5 ( $V_{\text{vir}} = 320 \text{ km s}^{-1}$ ) simulation.

We generalize the results from Hopkins et al. (2005a) and those above (which use simulation A3) to a range of masses, using the simulations A1, A2, A4, and A5. Recall, these simulations are identical except for increasing galaxy mass given by the sequence in virial velocity,  $V_{\text{vir}} = 80, 113, 160, 226,$  and  $320 \text{ km s}^{-1}$  for A1-A5, respectively. The evolution of these simulations would be simply related if not for the scale-dependent physics of cooling, star formation, and black hole accretion and feedback. Figures 4 and 5 plot the bolometric luminosity of and column densities to the supermassive black hole as a function of simulation time, for the period shortly before and after the merger in simulations A4 and A5, respectively. This is presented in the style of Figure 2 from Hopkins et al. (2005a), which showed the same for A3. The median column densities and 25%-75% contours are indicated for the total average simulation density, and the calculated hot-phase density, as described in §2.2, along with the observed B-band luminosity using the median hot-phase  $N_{\text{HI}}$ . The final masses of the black holes are also shown, where

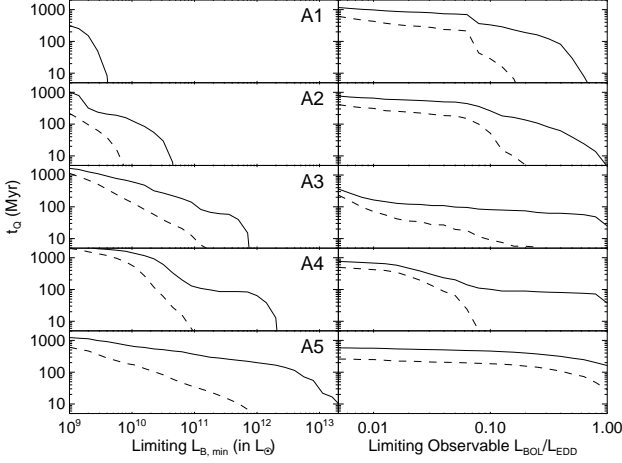


FIG. 6.— Left panels: Quasar lifetimes as a function of  $L_{B,\min}$  from the simulations (time with observed B-band luminosity  $L_{B,\text{obs}} \geq L_{B,\min}$ ). Results from simulations A1-A5 are shown from top to bottom. Solid lines indicate the lifetime if attenuation is ignored. The dashed lines give the median observed lifetime calculated with the metallicity-weighted, hot-phase neutral column density. Right panels: Same as the left panels, but with  $t_Q$  defined as a bolometric luminosity  $L_{\text{bol}} > lL_{\text{Edd}}$ , where the observable lifetime is the time above a given ratio  $l$  with B-band optical depth less than unity.

$M_{\text{BH, final}} \approx 7 \times 10^6, 3 \times 10^7, 3 \times 10^8, 7 \times 10^8,$  and  $2 \times 10^9$  for simulations A1-A5, respectively. The evolution seen in simulation A4 is quite similar to that of A3, with a sharp rise at the time of the merger to very large peak Eddington-limited luminosities, for a period  $\sim 10^8$  yr, much of which is unobservable in the optical owing to a corresponding rise in  $N_{\text{H1}}$ . At the final stages of strong accretion, when gas is rapidly being consumed and expelled, the observable luminosity finally rises to peak levels over a much shorter time interval  $\sim 10^7$  yr. In the A5 simulation, the period of rapid accretion and large, Eddington-limited intrinsic luminosities is significantly longer,  $\sim 3 \times 10^8$  yr, and the peak luminosity is higher, as expected. However, as before, most of this period is obscured by large column densities, and, remarkably, once again only the final stages of intrinsically high luminosity are visible, as gas is expelled and the accretion rate and column density both fall. The same behavior is seen in the A1 and A2 cases, though with much lower peak bolometric luminosities  $\sim 10^{10}$  and  $10^{11} L_{\odot}$ , respectively. The striking similarity of this process across all our simulations suggests that it is at least qualitatively insensitive to the details of the accretion history and galaxy or black hole masses.

We quantify the resulting quasar lifetimes in Figure 6, where we plot the quasar lifetime  $t_Q$  as a function of the limiting B-band luminosity  $L_{B,\min}$ . The panels show the lifetimes for simulations A1-A5, from top to bottom. In each panel, the solid curve shows the intrinsic lifetime  $t_Q^i$ ; i.e. the total time the intrinsic  $L_B \geq L_{B,\min}$ . The dashed curves show the integrated time that the observed B-band luminosity meets this criterion, using the median metallicity-weighted hot-phase neutral column density of the simulation (case C of Figure 1). As demonstrated in Figure 1 and in Hopkins et al. (2005a), varying this definition of the column density over realistic ranges can change the intrinsic lifetime by a factor of  $\sim 2-3$  at a given  $L_{B,\min}$ . We also plot the lifetime as a function of  $l$ , the ratio of the bolometric luminosity to the Eddington luminosity, and find a similar trend. Here, we calculate the “observed” time above a given ratio  $l$  as the time above such a ra-

tio with a B-band optical depth less than unity. In all cases, the observed  $t_Q$  is significantly smaller than the intrinsic lifetime for all  $L_{B,\min} > 10^9 L_{\odot}$ , and the ratio  $t_Q/t_Q^i$  decreases with increasing  $L_{B,\min}$ . However, both the intrinsic and observed lifetimes increase systematically at a given  $L_B > 10^9 L_{\odot}$  with increasing galaxy and black hole mass, and the peak luminosity similarly increases, as expected. In all cases corresponding to quasar-like luminosities, our estimates of observed lifetimes of  $\sim 10^7$  yr agree well with observations, with much longer intrinsic lifetimes  $\gtrsim 10^8$  yr.

A quasar accreting and radiating at the Eddington limit, with luminosity increasing exponentially up to some peak luminosity  $L_{\text{max}}$  after which accretion shuts off, will spend an integrated time above a given luminosity  $L$  given by

$$t_Q(L' > L) = t_S \ln(L_{\text{max}}/L), \quad (1)$$

where  $t_S$  is the Salpeter time,  $t_S = M_{\text{BH}}/\dot{M} = 4.5 \times 10^7$  yr at the Eddington rate with our efficiency  $\epsilon_r = 0.1$ , and  $L_{\text{max}}$  is given by the Eddington luminosity of the final black hole mass. This lifetime agrees well with the plotted lifetimes for simulations A3, A4, and A5 at the high-luminosity end. However, simulations A1 and A2 do not radiate at their Eddington limits for a long period of time, and the slope of this relation is too shallow in all cases, underpredicting the time that the simulation spends at luminosities  $L \lesssim 0.1 L_{\text{max}}$ . This is because the black holes in the simulations spend significant time at lower Eddington ratios both going into and coming out of the quasar stage and in an extended quiescent phase. Moreover, the observed lifetimes do not at all correspond to the lifetimes predicted by this simple model. Therefore, to simply describe the intrinsic and observed lifetimes as a function of limiting luminosity and final black hole mass (or peak luminosity  $L_{\text{max}}$ ), we fit the calculated lifetimes  $t_Q$  to truncated power laws, from  $L = 10^9 L_{\odot}$  to approximately  $0.5 L_{\text{max}}$ , or where  $t_Q \lesssim 1$  Myr, whichever occurs first. Thus we fit to the form

$$t_Q(L' > L) = t_9 (L/L_9)^{\alpha}, \quad (2)$$

where  $L_9 \equiv 10^9 L_{\odot}$  and  $t_9 = t_Q(L' > L_9)$ .

Figure 7 shows the resulting power-law slopes  $\alpha$  and normalizations  $t_9$  of the lifetimes  $t_Q$  as a function of the final black hole mass (or equivalently, the peak quasar luminosity given as the Eddington luminosity of the final black hole mass). The calculated, fitted, and Eddington-limit approximated lifetimes are also shown for comparison for the A3 simulation. The lifetimes are well-fitted by power laws in this range, and the discrepancy between the power-law and Eddington-limit approximated lifetimes at lower luminosities is clear. The slope of both the intrinsic and observed lifetimes becomes shallower at higher black hole masses, as the lifetime increases for all luminosities and extends to higher peak luminosities, but the slope of the observed lifetime evolves much more rapidly than the slope of the intrinsic lifetime. Over the range of our simulations, the intrinsic lifetime slope can be approximated as  $\alpha = -0.79 + 0.32 \log(M_{\text{BH}}/10^8 M_{\odot})$ , or  $\alpha = -0.95 + 0.32 \log(L_{\text{max}}/10^{12} L_{\odot})$ . Although the fluctuation in the normalization  $t_9$  is large for observed lifetimes, there does not appear to be a systematic trend with final black hole mass, which is expected as by luminosities of this level or lower, the lifetime is dominated by the quiescent-phase lifetime throughout the duration of the simulation. This is especially clear in the normalization of the intrinsic lifetimes, which also show no systematic trend and are all within a factor of  $\sim$  two of 2 Gyr, the approximate total duration of the simulations.

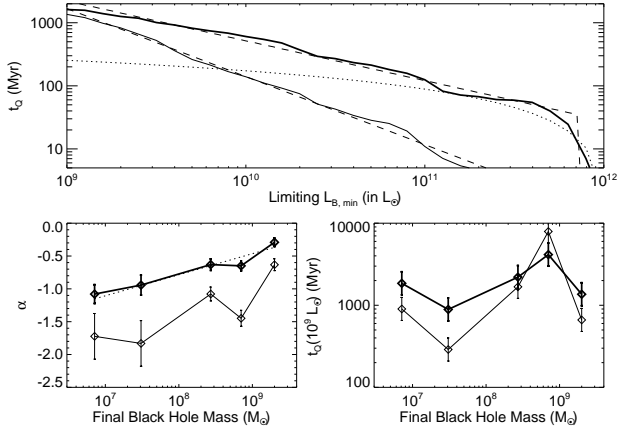


FIG. 7.— The results of fitting quasar lifetimes  $t_Q$  to truncated power laws of the form  $t_Q(L' > L) \propto L^\alpha$ . Upper panel shows the intrinsic (thick solid line) and observed (thin solid line) lifetimes in the A3 simulation, with dashed lines indicating the corresponding best-fit truncated power laws. The dotted line shows the lifetime expected for Eddington-limited accretion up to the final black hole mass. The lower panels plot the power law slopes  $\alpha$  and normalizations at  $L = 10^9 L_\odot$  of the power law fits to the intrinsic (thick) and observed (thin) lifetimes from the series of simulations A1-A5, as a function of the final black hole mass in the simulation. The dotted line in the left panel gives a simple linear fit to  $\alpha$  as a function of the logarithm of the final black hole mass.

In order to obtain a lower limit to quasar lifetimes at low luminosities, we repeat this analysis, but ignore all times prior to the intrinsically bright quasar phase (essentially the final merger). This excludes the luminosity of the black hole as it grows from its small seed mass, and ignores the periods of accretion with high gas fractions early in the merger, giving a lower limit corresponding to an already-large black hole suddenly “turning on” in a quasar phase. As expected, the Eddington-limited phase of the lifetime is more dominant in this case. However, the pure Eddington-limited model still gives lifetimes too short by an order of magnitude at low luminosities. Fitting to power laws we find very similar relations to those shown in Figure 7, with slightly shallower slopes,  $\alpha = -0.61 + 0.30 \log(M_{\text{BH}}/10^8 M_\odot)$  for the intrinsic lifetime, and normalization  $t_9 \sim 1 \text{ Gyr}$ . We further fit one additional functional form to the intrinsic lifetimes, in which the lifetime follows the Eddington-limited shape for large luminosities, down to some luminosity  $L_{\text{break}}$ , and below this luminosity follows a power-law. This allows a continuous description of the lifetime, very accurate at both low and near-peak luminosities. For these fits, we find similar power-law slopes  $\alpha = -0.81 + 0.32 \log(M_{\text{BH}}/10^8 M_\odot)$ , with  $L_{\text{break}} \approx 0.025 L_{\text{bol, max}} \approx 0.14 L_{\text{B, max}}$  nearly constant. We also fit the lifetimes as a function of frequency for the representative visual wavelengths shown in Figure 2. Although, as expected from the figure, the observed lifetime slopes become slightly shallower and the intrinsic lifetime slopes become slightly steeper as the quasar is observed at redder wavelengths, the change with wavelength across this range is very small compared to the change with black hole mass. Moreover, the change in normalization  $t_9$  across visual wavelengths is consistent with zero. We therefore find that quasar lifetimes can be well approximated by simple power laws, where the power law slope depends on the final black hole mass or peak luminosity of a system, and find significantly longer lifetimes at low luminosities than predicted by simple models of accretion at a constant Eddington ratio. Furthermore, attempts

to de-convolve intrinsic quasar properties and observations as well as semi-analytical attempts to model observable quasar luminosity functions and statistics require an accurate model of quasar lifetimes as a function of luminosity and host system properties. The fits we describe have the advantage of a simple, analytical form which can be applied to a continuum of luminosities and intrinsic quasar properties, while addressing the shortcomings of simpler lifetime models below peak system luminosities.

## 6. DISCUSSION & CONCLUSIONS

In this paper, we have studied implications of the conclusion of Hopkins et al. (2005a) that incorporating the effects of obscuration in a galaxy merger simulation gives observed quasar lifetimes of  $\sim 10^7 \text{ yr}$ . We extended our analysis to a series of five simulations with virial velocities  $V_{\text{vir}} = 80 - 320 \text{ km s}^{-1}$ , producing a range of final black hole masses from  $\sim 7 \times 10^6 - 2 \times 10^9 M_\odot$ , and find qualitatively similar results in all cases and for different determinations of the obscuring column density. The good agreement with observations and the significant difference between observed and much longer intrinsic lifetimes is found in all our simulations. The qualitative evolution of quasars in this model is robust, with the result reproduced across a range of galaxy masses, and using different methods for calculating column densities that can give factors greater than an order of magnitude different attenuations along any given line of sight at a particular time. We therefore expect that quasars will have extended intrinsic lifetimes, much of which are obscured in visual wavelengths. The processes which fuel periods of quasar activity by channeling significant quantities of gas into the central regions of a galaxy will produce this extended intrinsic lifetime of  $\gtrsim 10^8 \text{ yr}$ . However, for a significant fraction of the intrinsic lifetime for quasar activity, this same process will produce large column densities which heavily obscure the quasar and attenuate it well below observable limits in the B-band and other visual wavelengths. Eventually, feedback from accretion energy will remove surrounding gas, creating a window in which the quasar is optically observable before accretion rates drop below those needed to maintain quasar luminosities.

We do not expect other considerations, such as the orbital parameters of the merger or the collimation of black hole feedback, to substantially change our results. Different orbital separations, orientations, and energies will change the time of interaction, but ultimately our model for quasar evolution depends only on the merger eventually depositing sufficient gas into the central regions of the remnant to fuel rapid black hole growth. After such a process begins, the evolution of the black hole should be determined by the self-regulated mechanisms which terminate black hole growth, as described in Di Matteo et al. (2005). This will eventually expel gas, rendering the quasar observable and shutting down the accretion phase at the final black hole mass given by the  $M_{\text{BH}}-\sigma$  relation. The phase of rapid black hole growth and the expulsion of gas in the final stages of strong accretion occur during the end-stages of the merger and in the very center of the merging cores, when and where the structure of the original orbits should be least important. This view is supported by additional simulations not presented here but shown in e.g. Fig. 16 of Springel et al. (2005b), demonstrating that the final black hole mass is relatively insensitive to orbital parameters.

The exact mechanism of black hole feedback should similarly not dramatically change this picture, so long as a pe-

riod of rapid black hole growth occurs, requiring large densities (which naturally generate obscuring column densities), and ultimately terminates via some self-regulated mechanism which expels gas from central regions, rendering the quasar optically observable in the final stages of its life. In particular, collimation of the black hole feedback may significantly increase the energy or momentum input on-axis, “blowing out” material along this axis earlier in the quasar lifetime. However, since the black hole is growing exponentially during peak accretion, this should occur at most on the order of a couple of Salpeter times (during which the black hole luminosity grows by an order of magnitude) before it would in the isotropic case, changing the intrinsic lifetime by only a fraction of its total. The unobscured stage of the quasar lifetime may then begin slightly earlier along on-axis sightlines, but should be of comparable duration as a similar mechanism removes the gas from central regions. In addition, in order for significant black hole growth to cease at the same critical mass as in the isotropic case (determined by the  $M_{\text{BH}}-\sigma$  relation), the high-accretion rate phase must end over the same timescale  $\sim t_S$  as the “lead” with which collimated, on-axis blowout precedes isotropic blowout. The necessity that self-regulation eventually terminates accretion implies that surrounding densities, even off-axis, must decrease, resulting in at most a broadening of the column density distribution as typical column densities off-axis could be somewhat larger than column densities on-axis.

For much of this regime, we find that the source should be observable in hard X-ray frequencies, as the attenuation is weaker and column densities generally lie below the Compton thick limit. This distinction naturally produces a substantial population of obscured quasars, as a standard phase in the evolution of quasars over their lifetimes. Although we defer a detailed calculation of the quasar luminosity function as a function of redshift and in different observed frequencies (Hopkins et al. 2005b), we note that such a population can naturally account for both the cosmic X-ray background spectrum and discrepancies between optical and X-ray luminosity functions at various redshifts (Hopkins et al. 2005c). Moreover, optical and X-ray observational samples will be affected rather differently by selection effects and magnitude limits, especially for quasars near their peak luminosities. Therefore, the differences in the evolution of optical and X-ray selected samples may be accounted for through the dependence of obscuration on intrinsic luminosity and host galaxy properties. Attenuation is also weaker in the infrared, and the large fraction of optical and UV energy absorbed during the obscured phase may be reprocessed by dust, appearing as thermal radiation in the IR. This may render the observable lifetime larger than the intrinsic lifetime at long wavelengths, an effect important for calculating the IR background and estimating source populations. Similarly, the total obscuration and obscuration as a function of intrinsic luminosity are important for the evolution of luminous and ultraluminous infrared galaxies, and for estimating the relative energy contributions in the IR of starbursts and active galactic nuclei (AGN).

The typical column densities in our simulations correspond well to observed column densities of optically selected quasars, once the appropriate observed magnitude limit has been imposed. Thus, our model allows us to reproduce the distribution of optically obscured sources above this magnitude limit naturally, as an evolutionary effect of the mechanisms which fuel and regulate quasar growth, without invoking particular distributions of source properties or geometric

patterns of obscuration. Moreover, the column densities we calculate in our simulations allow us to predict that the distribution of  $N_{\text{H}}$  values should become broader as the minimum observable luminosity is decreased, as both faint, quiescent phases with low ( $\lesssim 10^{20} \text{ cm}^{-2}$ ) column densities and bright, obscured phases with high ( $\gtrsim 10^{22} \text{ cm}^{-2}$ ) column densities become observable. This effect is seen in the broad distribution of  $N_{\text{H}}$  values in X-ray samples, which are much less affected by attenuation, but a more detailed analysis including modeling the distribution of quasar properties is needed to reproduce both the optical and X-ray  $N_{\text{H}}$  distributions more accurately.

We find that the peak luminosities and lifetime above any given luminosity increase systematically with galaxy mass and final black hole mass, although the distinction between observed and intrinsic lifetimes remains significant in all cases. Moreover, the ratio of observed to intrinsic lifetimes decreases in all cases with increasing minimum luminosity. We also find that intrinsic lifetimes at luminosities  $\lesssim 0.1$  times the peak luminosity are poorly fit by assuming quasars always accrete near the Eddington limit, but rather that lifetimes are well-fitted by power laws with a steeper slope. This is a result of sub-Eddington accretion rates both before and after the peak accretion phase, even at luminosities significantly above the quiescent steady-state small accretion rates seen at late times in the simulations. This suggests that many quasars seen at low luminosities may be quasars with a large peak luminosity in a significantly sub-Eddington phase, although the fraction of quasars observed at high Eddington ratios becomes large with increasing luminosity.

Additionally, these lifetimes imply that, even at high luminosities where growth may be Eddington-limited, quasars spend a significant fraction of their lives with intrinsic luminosities well below their peak luminosities. Therefore, any observed luminosity function is the convolution of the distribution of quasars with a given peak luminosity (determined by the final black hole mass and thus the merging galaxy properties) and a non-trivial light curve (Hopkins et al. 2005b). It is clear from these calculations that any attempt to theoretically model even the intrinsic luminosity functions of quasars must take into account the functional dependence of the light curve on luminosity and time. In order to apply these models to observed luminosity functions, the dependence of observed luminosity on intrinsic luminosity and the quasar evolution, as well as the observed frequency, must be considered (Hopkins et al. 2005b,c).

We find that the ratio of observable to intrinsic lifetimes is a strongly decreasing function of the limiting luminosity of observations. Modeling this effect is necessary to estimate intrinsic quasar lifetimes from observations, as well as for using theoretically motivated accretion models to predict the quasar luminosity function and space density of present-day supermassive black holes. Further, the effects we describe can account for the presence of an obscured population of quasars which are missed by optical, UV, or soft X-ray surveys but may contribute significantly to the cosmic X-ray background. Observations of the cosmic X-ray background and comparison of the optical and hard X-ray quasar luminosity functions that indicate the existence of a large obscured population of quasars (Brandt & Hasinger 2005, and references therein), is explained in our picture, because it predicts different observed lifetimes and populations at different frequencies. The scenario we describe also implies that the reprocessing of quasar radiation by dust in surrounding regions can account for ob-

servations of luminous and ultraluminous infrared galaxies with merger activity and obscured AGN.

Together with the modeling presented by Di Matteo et al. (2005), Springel et al. (2005a,b), Springel & Hernquist (2005), Hopkins et al. (2005a,b,c), and Robertson et al. (2005), the results described here motivate the following picture for galaxy formation and evolution. Through the hierarchical growth of structure in a cold dark matter universe (White & Rees 1978), mergers between galaxies occur on a regular basis. Those involving gas-rich progenitors, which would be increasingly more common towards higher redshifts, produce inflows of gas through gravitational torques (Barnes & Hernquist 1991, 1996), causing starbursts (Mihos & Hernquist 1994, 1996) like those associated with luminous infrared galaxies (e.g. Sanders & Mirabel 1996). The high gas densities triggering these starbursts fuel rapid black hole growth. For most of the period over which black hole growth occurs, optical quasar activity would be buried, but X-rays from the black holes explain the presence of non-thermal point sources in e.g. NGC 6240 (Komossa et al. 2003), and reprocessing of most of the black hole energy by surrounding gas and dust can, in principle, account for the spectral energy distributions of “warm” ULIRGs (Sanders et al. 1988c) and recent observations of a correlation between quasar obscuration and far-infrared host luminosity

(e.g., Page et al. 2004; Stevens et al. 2005). As the black hole mass and radiative output increase, a critical point is reached where feedback energy starts to expel the gas fueling accretion. For a relatively brief period of time, the galaxy would be seen as an optical quasar with a B-band luminosity and lifetime characteristic of observed quasars. This phase of evolution is brief ( $\sim 10^7$  yr), owing to the explosive nature of the final stages of black hole growth as the gas responds dramatically to the feedback energy from the exponentially evolving black hole. This AGN feedback terminates further black hole growth, leaving a remnant that resembles an ordinary galaxy containing a dead quasar and satisfying the  $M_{\text{BH}}-\sigma$  relation. Modeling both the dependence of quasar lifetime on luminosity, and the complex, time-dependent evolution of quasar obscuration is thus crucial to any observational or theoretical understanding of quasars and quasar host galaxy evolution.

This work was supported in part by NSF grants ACI 96-19019, AST 00-71019, AST 02-06299, and AST 03-07690, and NASA ATP grants NAG5-12140, NAG5-13292, and NAG5-13381. The simulations were performed at the Center for Parallel Astrophysical Computing at the Harvard-Smithsonian Center for Astrophysics.

#### REFERENCES

- Allen, D.A., Roche, P.F. & Norris, R.P. 1985, MNRAS, 213, 67p  
 Armus, L., Heckman, T.M. & Miley, G. 1987, AJ, 94, 831  
 Bahcall, J.N., Kirhakos, S. & Schneider, D.P. 1994, ApJ, 435, L11  
 Bahcall, J.N., Kirhakos, S. & Schneider, D.P. 1995, ApJ, 450, 486  
 Bajdik, S., Duncan, R. C., & Ostriker, J. P. 1988, ApJ, 327, 570  
 Barnes, J. E. 1988, ApJ, 331, 699  
 Barnes, J. E. 1992, ApJ, 393, 484  
 Barnes, J. E. & Hernquist, L. 1991, ApJ, 370, L65  
 Barnes, J. E. & Hernquist, L. 1992, ARA&A, 30, 705  
 Barnes, J. E. & Hernquist, L. 1996, ApJ, 471, 115  
 Bouchet, P., Lequeux, J., Maurice, E., Prevot, L., & Prevot-Burnichon, M. L. 1985, A&A, 149, 330  
 Brandt, W.N., Hasinger G., 2005, ARA&A, in press  
 Brotherton, M. S., Tran, H. D., Becker, R. H., Gregg, M. D., Laurent-Muehleisen, S. A., & White, R. L. 2001, ApJ, 546, 775  
 Busha, M.T., Evrard, A.E., Adams, F.C. & Wechsler, R.H. 2004, MNRAS, submitted [astro-ph/0412161]  
 Canalizo, G. & Stockton, A. 2001, ApJ, 555, 719  
 Ciotti, L. & Ostriker, J. P. 1997, ApJ, 487, L105  
 Ciotti, L. & Ostriker, J. P. 2001, ApJ, 551, 131  
 Croft, R. A. C. 2004, ApJ, 610, 642  
 Davé, R., Hernquist, L., Katz, N. & Weinberg, D.H. 1999, ApJ, 511, 521  
 Di Matteo, T., Croft, R. A. C., Springel, V., & Hernquist, L. 2003, ApJ, 593, 56  
 Di Matteo, T., Croft, R. A. C., Springel, V., & Hernquist, L. 2004, ApJ, 610, 80  
 Di Matteo, T., Springel, V., & Hernquist, L. 2005, Nature, 433, 604  
 Elvis, M., et al. 1994, ApJS, 95, 1  
 Fabian, A. C. 1999, MNRAS, 308, L39  
 Ferrarese, L. & Merritt, D. 2000, ApJ, 539, L9  
 Francis, P. J., Drake, C. L., Whiting, M. T., Drinkwater, M. J., & Webster, R. L. 2001, Publications of the Astronomical Society of Australia, 18, 221  
 Gebhardt, K., Bender, R., Bower, G. et al. 2000, ApJ, 539, L13  
 George, I. M., Turner, T. J., Netzer, H., Nandra, K., Mushotzsky, R. F., & Yaqoob, T. 1998, ApJS, 114, 73  
 Gerssen, J. et al. 2004, AJ, 127, 75  
 Granato G.L., De Zotti G., Silva L., Bressan A., Danese L., 2004, ApJ, 600, 580  
 Grazian, A., Negrello, M., Moscardini, L., Cristiani, S., Haehnelt, M. G., Matarrese, S., Omizzolo, A., & Vanzella, E. 2004, AJ, 127, 592  
 Greenstein, J.L. & Mathews, T.A. 1963, Nature, 197, 1041  
 Gregg, M. D., Lacy, M., White, R. L., Glikman, E., Helfand, D., Becker, R. H., & Brotherton, M. S. 2002, ApJ, 564, 133  
 Haehnelt, M. G., Natarajan, P., & Rees, M. J. 1998, MNRAS, 300, 817  
 Haiman, Z. & Cen, R. 2002, ApJ, 578, 702  
 Heckman, T. M., Bothun, G. D., Balick, B., & Smith, E. P. 1984, AJ, 89, 958  
 Hernquist, L. 1989, Nature, 340, 687  
 Hernquist, L. 1990, ApJ, 356, 359  
 Hernquist, L. 1992, ApJ, 400, 460  
 Hernquist, L. 1993, ApJ, 409, 548  
 Hernquist, L. & Mihos, J.C. 1995, ApJ, 448, 41  
 Hopkins, P.F., Hernquist, L., Martini, P., Cox, T. J., Robertson, B., Di Matteo, T., & Springel, V. 2005a, ApJ, submitted [astro-ph/0502241]  
 Hopkins, P. F., Hernquist, L., Cox, T. J., Robertson, B., Di Matteo, T., & Springel, V. 2005b, ApJ, submitted  
 Hopkins, P. F., Hernquist, L., Cox, T. J., Robertson, B., Di Matteo, T., & Springel, V. 2005c, ApJ, submitted  
 Hopkins, P. F., Strauss, M. A., Hall, P. B., Richards, G. T., Cooper, A. S., Schneider, D. P., Vanden Berk, D. E., Jester, S., Brinkmann, J., & Szokoly, G. P. 2004, AJ, 128, 1112  
 Hutchings, J. B., & Neff, S. G. 1992, AJ, 104, 1  
 Jakobsen, P., Jansen, R. A., Wagner, S., & Reimers, D. 2003, A&A, 397, 891  
 Jogee, S. 2004, in AGN Physics on All Scales, in press [astro-ph/0408383]  
 Joseph, R.D. & Wright, G.S. 1985, MNRAS, 214, 87  
 Katz, N., Weinberg, D.H. & Hernquist, L. 1996, ApJS, 105, 19  
 Kauffmann, G. & Haehnelt, M. 2000, MNRAS, 311, 576  
 Kleinmann, S.G. et al. 1988, ApJ, 328, 161  
 Komossa, S., Burwitz, V., Hasinger, G., Predehl, P., Kaastra, J. S., & Ikebe, Y. 2003, ApJ, 582, L15  
 Lynden-Bell, D. 1969, Nature, 223, 690  
 Magorrian, J. et al. 1998, AJ, 115, 2285  
 Marconi, A., Risaliti, G., Gilli, R., Hunt, L. K., Maiolino, R., & Salvati, M. 2004, MNRAS, 351, 169  
 Martini, P. 2004, in Carnegie Obs. Astrophys. Ser. 1, Coevolution of Black Holes and Galaxies, ed. L.C. Ho (Cambridge: Cambridge Univ. Press), 170  
 Mathews, T.A. & Sandage, A.R. 1963, ApJ, 138, 30  
 Max, C.E. et al. 2005, ApJ, in press [astro-ph/0411590]  
 McKee, C. F. & Ostriker, J. P. 1977, ApJ, 218, 148  
 Mihos, J. C. & Hernquist, L. 1994, ApJ, 437, 611  
 Mihos, J. C. & Hernquist, L. 1996, ApJ, 464, 641  
 Morrison, R. & McCammon, D. 1983, ApJ, 270, 119  
 Navarro, J. F., Frenk, C. S., White S. D. M., 1996, ApJ, 462, 563  
 Page, M. J., Stevens, J. A., Ivison, R. J., & Carrera, F. J. 2004, ApJ, 611, L85  
 Pei, Y. C. 1992, ApJ, 395, 130  
 Perola, G. C., Matt, G., Cappi, M., Fiore, F., Guainazzi, M., Maraschi, L., Petrucci, P. O., & Piro, L. 2002, A&A, 389, 802  
 Porciani, C., Magliocchetti, M., & Norberg, P. 2004, MNRAS, 355, 1010  
 Richards, G. T., Fan, X., Schneider, D. P., Vanden Berk, D. E., Strauss, M. A., York, D. G., Anderson, J. E., Anderson, S. F., et al. 2001, AJ, 121, 2308

- Rines K., Geller M. J., Diaferio A., Kurtz M. J., Jarrett T. H., 2004, *AJ*, 128, 1078
- Rines K., Geller M. J., Diaferio A., Mahdavi A., Mohr J. J., Wegner G., 2002, *AJ*, 124, 1266
- Rines K., Geller M. J., Diaferio A., Mohr J. J., Wegner G. A., 2000, *AJ*, 120, 2338
- Rines K., Geller M. J., Kurtz M. J., Diaferio A., 2003, *AJ*, 126, 2152
- Robertson, B., Yoshida, N., Springel, V., & Hernquist, L. 2004, *ApJ*, 606, 32
- Robertson, B., Hernquist, L., Bullock, J.S., Cox, T.J., Di Matteo, T., Springel, V., & Yoshida, N. 2005, *ApJ*, submitted
- Salpeter, E. E. 1964, *ApJ*, 140, 796
- Sanders, D.B. et al. 1986, *ApJ*, 305, L45
- Sanders, D.B. et al. 1988a, *ApJ*, 325, 74
- Sanders, D.B. et al. 1988b, *ApJ*, 324, L55
- Sanders, D.B. et al. 1988c, *ApJ*, 328, L35
- Sanders, D. B. & Mirabel, I. F. 1996, *ARA&A*, 34, 749
- Sargent, A.I. et al. 1987, *ApJ*, 312, L35
- Sargent, A.I., Sanders, D.B. & Phillips, T.G. 1989, *ApJ*, 346, L9
- Schmidt, M. 1963, *Nature*, 197, 1040
- Scoville, N.Z. et al. 1986, *ApJ*, 311, L47
- Silk, J. & Rees, M. J. 1998, *A&A*, 331, L1
- Soifer, B.T. et al. 1984a, *ApJ*, 278, L71
- Soifer, B.T. et al. 1984b, *ApJ*, 283, L1
- Soifer, B.T., Houck, J.R. & Neugebauer, G. 1987, *ARA&A*, 25, 187
- Sokasian, A., Abel, T., & Hernquist, L. 2002, *MNRAS*, 332, 601
- Sokasian, A., Abel, T., & Hernquist, L. 2003, *MNRAS*, 340, 473
- Soltan, A. 1982, *MNRAS*, 200, 115
- Springel, V., Di Matteo, T., & Hernquist, L. 2005a, *ApJ*, submitted, [astro-ph/0409436]
- Springel, V., Di Matteo, T., & Hernquist, L. 2005b, *MNRAS*, submitted, [astro-ph/0411108]
- Springel, V. & Hernquist, L. 2002, *MNRAS*, 333, 649
- Springel, V. & Hernquist, L. 2003, *MNRAS*, 339, 289
- Springel, V. & Hernquist, L. 2005, *ApJ*, in press [astro-ph/0411379]
- Springel, V., Yoshida, N., & White, S. D. M. 2001, *New Astronomy*, 6, 79
- Stevens, J. A., Page, M. J., Ivison, R. J., Carrera, F. J., Mittaz, J. P. D., Smail, I., & McHardy, I. M. 2005, *MNRAS*, submitted, [astro-ph/0503618]
- Stockton, A. 1978, *ApJ*, 223, 747
- Stockton, A. & MacKenty, J. 1987, *ApJ*, 316, 584
- Stockton, A. & Ridgway, S. 1991, *AJ*, 102, 488
- Telfer, R. C., Zheng, W., Kriss, G. A., & Davidsen, A. F. 2002, *ApJ*, 565, 773
- Toomre A., 1977, in *Evolution of Galaxies and Stellar Populations*, 401, Yale Univ. Obs: New Haven
- Toomre A. & Toomre J., 1972, *ApJ*, 178, 623
- Ueda, Y., Akiyama, M., Ohta, K., & Miyaji, T. 2003, *ApJ*, 598, 886
- Vanden Berk, D. E., et al. 2001, *AJ*, 122, 549
- Vignali, C., Brandt, W. N., & Schneider, D. P. 2003, *AJ*, 125, 433
- Webster, R. L., Francis, P. J., Peterson, B. A., Drinkwater, M. J., & Masci, F. J. 1995, *Nature*, 375, 469
- White, R. L., Helfand, D. J., Becker, R. H., Gregg, M. D., Postman, M., Lauer, T. R., & Oegerle, W. 2003, *AJ*, 126, 706
- White, S.D.M. & Rees, M.J. 1978, *MNRAS*, 183, 341
- Wyithe, J. S. B. & Loeb, A. 2002, *ApJ*, 581, 886
- Wyithe, J. S. B. & Loeb, A. 2003, *ApJ*, 595, 614
- Yu, Q. & Lu, Y. 2004, *ApJ*, 602, 603
- Yu, Q. & Lu, Y. 2005, *ApJ*, in press [astro-ph/0411098]
- Yu, Q. & Tremaine, S. 2002, *MNRAS*, 335, 965
- Zel'dovich, Ya.B. & Novikov, I.D. 1964, *Sov. Phys. Dokl.* 158, 811